A neutron scattering study of the impulse approximation in single-crystal beryllium

1990 J. Phys.: Condens. Matter 2 1045

(http://iopscience.iop.org/0953-8984/2/5/001)

J. Phys.: Condens. Matter **2** (1990) 1045–1057. Printed in the UK

A neutron scattering study of the impulse approximation in single-crystal beryllium

D F McMorrow†, R A Cowley†‡, R M Nicklow§, P W Mitchell‖, A D Taylor¶ and M Mostoller§

† Department of Physics, University of Edinburgh, Mayfield Road, Edinburgh EH9 3JZ, UK
§ Oak Ridge National Laboratory, Oak Ridge, TN 37831, USA
‖ Department of Physics, Schuster Laboratory, The University, Manchester M13 9PL, UK
¶ Rutherford Appleton Laboratory, Chilton, Didcot, Oxon OX11 0QX, UK

Received 19 May 1989, in final form 9 October 1989

Abstract. The inelastic scattering of high-energy neutrons from a single crystal of beryllium has been measured in order to test the validity of the impulse approximation. Separate measurements were performed, all with the sample at room temperature, with the wave-vector transfer along ⟨100⟩, ⟨110⟩ and ⟨001⟩ using the time-of-flight spectrometer HET at ISIS. For wave-vector transfers $\geqslant 35$ Å^{-1}, corresponding to an incident neutron energy of $\simeq 1$ eV, we find that the scattering is centred at the recoil energy given by the impulse approximation. Also, in this regime, the width is independent of the orientation of the wave-vector transfer with respect to the crystal axes and has a value consistent with that expected from a harmonic model of beryllium. We show that our experimental criterion for the validity of the impulse approximation is in agreement with a numerical calculation of the asymptotic behaviour of the exact incoherent neutron dynamic structure factor.

1. Introduction

The interest in determining the momentum distribution of atoms in condensed matter systems by neutron scattering has now spanned more than two decades. This followed from a proposal by Hohenberg and Platzman (1966) that the percentage of atoms in the zero-momentum superfluid state, the condensate fraction, of ^{4}He could be directly measured using high-energy neutrons. In their analysis of the neutron scattering cross-section they assumed that coherent effects are negligible and that after being struck by a neutron the target atom recoils as if it were free. The dynamical structure factor resulting from these assumptions is now referred to as the impulse approximation. It is directly related to the single-particle momentum distribution $n(\boldsymbol{p})$ by

$$S_{\mathrm{IA}}(\boldsymbol{Q}, \omega) = \int \mathrm{d}\boldsymbol{p}\, n(\boldsymbol{p}) \delta \left(\hbar\omega - \hbar\omega_{\mathrm{r}} - \left(\frac{\hbar^2}{M} \right) \boldsymbol{Q} \cdot \boldsymbol{p} \right) \tag{1}$$

where $\boldsymbol{Q}$ is the wave-vector transfer, $E_{\mathrm{r}} = \hbar\omega_{\mathrm{r}} = \hbar^2 Q^2 / 2M$ is the recoil energy, M is the

‡ Present address: Clarendon Laboratory, Parks Road, Oxford OX1 3PU, UK.

0953-8984/90/051045 + 13 $03.50

mass of the target atom and all other symbols have their usual meaning (see, for example, Hilleke *et al* 1984).

The impulse approximation is known to be exact as $Q \rightarrow \infty$ (Sears 1969), other than for systems with perfectly hard-core potentials (Weinstein and Negele 1982). At finite values of Q there are corrections to the impulse approximation arising from the fact that the target atom does not recoil freely, but interacts with its neighbouring atoms. Although many papers have appeared in the literature on the effect of these final-state interactions (see, for example, Sears (1984) and Silver (1988)), currently no exact theory exists. This is of critical importance in the case of superfluid ^{4}He, as the method used to correct the data for final-state interactions affects the value obtained for the condensate fraction. Moreover, the fact that the well-defined condensate peak predicted by Hohenberg and Platzman (1966) has never been observed is attributed to final-state interactions. Qualitatively, final-state interactions introduce an asymmetry into the measured lineshape as a function of ω, such that the high-energy tails are enhanced and the low-energy tails depressed. In addition, the centre of the scattered neutron distribution is shifted to an energy lower than the nominal recoil energy E_r, and the variance reduced from the value given by the impulse approximation (see, for example, Sears 1984).

In contrast to the numerous studies of the validity of the impulse approximation in quantum fluids, very few experimental results have been reported for crystalline solids. This situation is likely to change in the near future, as experiments requiring large neutron energy and wave-vector transfers can now be performed in reasonable times on the new spallation sources around the world. From a theoretical standpoint, one attractive feature of studying crystalline solids is that their lattice dynamics can often be adequately treated within the harmonic approximation, which leads to a particularly simple form of the impulse approximation. Also, within the harmonic approximation, the exact incoherent dynamical structure factor can be numerically calculated from the phonon density of states. Examples of experiments on crystalline solids performed at spallation sources include: a study of polycrystalline, HCP ^{4}He by Hilleke *et al* (1984), who used the impulse approximation to show that the momentum distribution is Gaussian, with a width slightly larger than the theoretical value; and more recently Hewitt *et al* (1989) found that the scattered neutron intensity from polycrystalline ^{6}Li was centred at the nominal recoil energy for wave-vector transfers greater than 45 Å^{-1}, but with a width significantly larger than that expected from a harmonic model of Li.

The aim of our study was to investigate whether the asymptotic region for the validity of the impulse approximation in beryllium can be reached using neutrons from a spallation source. For our measurements we used a single crystal as it was hoped that by orienting the wave-vector transfer along different crystallographic directions it would be possible to study any anisotropy in the final-state interactions. A simple picture of how this anisotropy arises is provided by considering how far a beryllium atom has to recoil after it has been struck by a neutron before 'colliding' with its nearest neighbour. In the HCP structure of beryllium, this distance is greatest for an atom recoiling along $\langle 001 \rangle$ and shortest for one recoiling along $\langle 100 \rangle$. Thus, naively at least it may be expected that final-state effects should be greater in the latter case than in the former. The other physical properties of beryllium which made it a suitable candidate for study include: its large neutron cross-section and high density both lead to a high count rate; its high Debye temperature (1000 K) means that it is effectively in its ground state at room temperature; and its light mass means that the recoil scattering is well separated from the phonons.

In the following section we consider the form of the impulse approximation as applied to a harmonic crystal, and indicate how the width of $S_{IA}(\boldsymbol{Q}, \omega)$ can be calculated from

the phonon density of states. We then describe in section 2.2 the method we used to generate the phonon density of states of beryllium by using a Born–von Karman model to fit the phonon dispersion relations measured by Steadman *et al* (1976). In section 2.3 we present a numerical calculation of the exact incoherent neutron dynamical structure factor for a harmonic solid and compare it with the impulse approximation result. The experimental details and results are given respectively in sections 3 and 4. Finally, in section 5 we discuss our experimental results with reference to the theory presented in section 2.

2. Theory

2.1. The impulse approximation for a harmonic crystal

In deriving the impulse approximation, coherent effects are neglected and it is assumed that after being struck by a neutron the target atom recoils as if it were free. For a harmonic solid, where the atoms are in potential wells from which they cannot be unbound, the second of these assumptions would appear to cause difficulties. It has been argued, however, by Gunn *et al* (1986) that the impulse approximation still works for such a system as long as the recoiling atom displays free-particle (plane-wave) behaviour in the region of space where the wavefunction of its initial state is significant. Moreover, a numerical study by Gunn and Warner (1984) showed that for a harmonic crystal the impulse approximation is approached at high wave-vector transfers.

For a harmonic solid, the impulse approximation gives for the dynamic structure factor the result

$$S_{\mathrm{IA}}(\boldsymbol{Q}, \omega) = [1/(2\pi\sigma^2)^{1/2}] \exp[-\tfrac{1}{2}(\hbar\omega - \hbar^2 Q^2/2M)^2/\sigma^2] \tag{2}$$

(Lovesey 1987). The dynamic structure factor is thus a Gaussian centred at the recoil energy E_{r} and of variance

$$\sigma^2 = (\hbar^2/M^2)\langle(\boldsymbol{Q}\cdot\hat{\boldsymbol{p}})^2\rangle \tag{3}$$

where $\hat{\boldsymbol{p}}$ is the momentum operator of the recoiling atom. Clearly, for a solid with an anisotropic momentum distribution the variance depends on the direction of the wave-vector transfer with respect to the crystal axes. We note in passing that, independently of either the impulse or harmonic approximations, the variance of the dynamic structure factor is rigorously related to the mean kinetic energy per particle, $\langle K\rangle$, by the second-moment sum rule, namely

$$\sigma^2 = \tfrac{4}{3}\langle K\rangle E_{\mathrm{r}}. \tag{4}$$

Thus, within the impulse approximation, the width and centre of the measured scattered neutron distribution are expected to scale respectively with Q and Q^2.

2.2. The phonon density of states

Although the phonon dispersion relations of beryllium have been measured in great detail by Steadman *et al* (1976), no attempt was made by them to calculate the phonon density of states. We have therefore fitted their data with a Born–von Karman force model. Our analysis was essentially the same as described by Houmann and Nicklow (1970), except that the present calculation was based on data for the high-symmetry

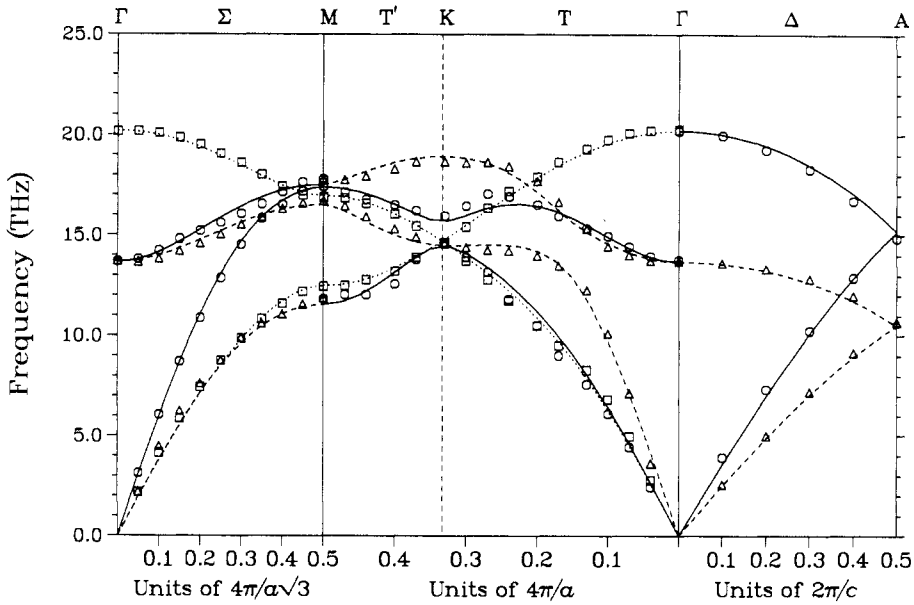

Figure 1. The phonon dispersion relations of beryllium for wave-vectors along the three high-symmetry directions. Data: taken from Steadman *et al* (1976); curves: obtained by fitting a Born–von Karman model to the data with forces extending to sixth-nearest neighbour.

directions and the AH, HL and AL edges of the zone boundary only. An excellent fit to all the measured frequencies was obtained for a model with forces extending to sixth-nearest neighbour, as shown in figure 1 for the high-symmetry directions. The force constants derived from the fit are listed in table 1.

We have made no study of the physical significance, or lack thereof, of this model. Rather our intention was to try to obtain the best overall description of the measured dispersion curves in order to calculate, with existing computer codes, the properties of the atomic motion which are relevant to this research and which depend only on averages over these curves. (Actually, for the purpose of this present work, as we will discuss below, the details of the model have negligible effect on our analysis.)

The normalised density of phonon states projected both parallel ($g_z(\omega)$) and perpendicular ($g_{xy}(\omega)$) to the $\boldsymbol{c}$ axis were then calculated using this model. The results are shown in figure 2(a) and 2(b). In addition we also calculated the temperature variation of the corresponding projections of the mean square atomic displacement $\langle u^2 \rangle$ and mean square momentum $\langle p^2 \rangle$. A reflection of the fact that our model is a reasonable representation of the dynamics of the beryllium atoms is that our calculated value of 0.00582 Å^{-2} for $\langle u^2 \rangle$ in the basal plane at 300 K is quite close to the value determined from neutron diffraction data of 0.00594(3) Å^{-2} (Larsen *et al* 1980). In figure 3 we present the results for the calculated thermal evolution of $\langle p^2 \rangle$, which was found to be isotropic to better than 1%, even at low temperatures, despite the visible differences in the densities of states shown in figure 2. Hence, within the harmonic approximation, the width of recoil scattering which is related through equation (3) to $\langle p^2 \rangle$ is also expected to be largely independent of the angle between $\boldsymbol{Q}$ and the crystallographic axes. The numerical value of the full width at half maximum (FWHM) in meV of $S_{IA}(\boldsymbol{Q}, \omega)$ for

Table 1. The real-space Born–von Karman force constants for beryllium as defined in Houmann and Nicklow (1970). For fifth and sixth neighbours, central forces are assumed, with the radial and tangential force constants defined respectively by $A(R) = V''(R)$ and $B(R) = V'(R)/R$.

Neighbour	Separation	Element	Value (dyn cm^{-1})
1	$(a/\sqrt{3}, 0, c/2)$	xx	13090
		yy	2820
		zz	19060
		$xz = +zx$	11440
2	$(0, a, 0)$	xx	2500
		yy	18820
		zz	830
		$xy = -yx$	5230
3	$(-2a/\sqrt{3}, 0, c/2)$	xx	1310
		yy	−1710
		zz	120
		$xz = +zx$	−6200
4	$(0, 0, c)$	xx	2520
		zz	4070
5	$(5a/2\sqrt{3}, a/2, c/2)$	$A(R)$	1650
		$B(R)$	120
6	$(a\sqrt{3}, 0, 0)$	$A(R)$	1850
		$B(R)$	510

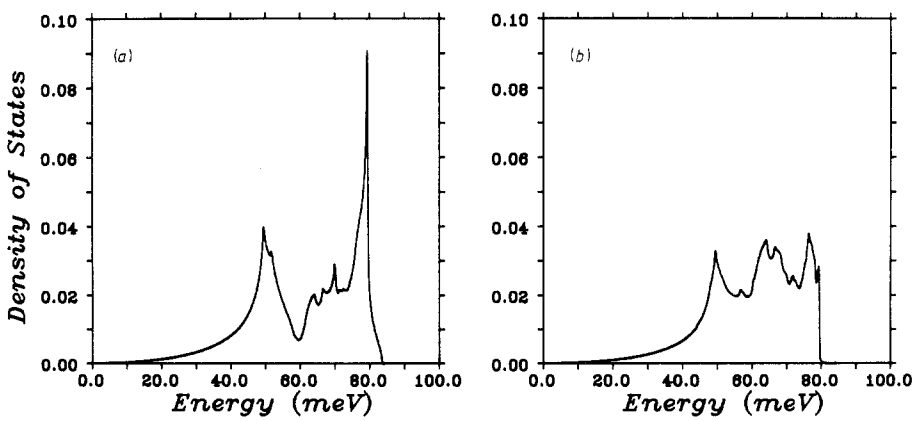

Figure 2. The normalised phonon density of states of beryllium generated by fitting the measured phonon dispersion relations with a Born–von Karman model (see text). (*a*) The phonon density of states $g_z(\omega)$ projected along **c**. (*b*) The phonon density of states $g_{xy}(\omega)$ projected in the basal plane.

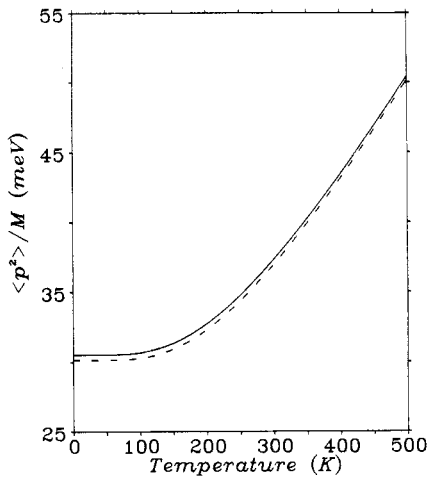

Figure 3. The calculated temperature dependence of the mean square phonon momentum $\langle p^2 \rangle$. The broken and full curves represent $\langle p_{xy}^2 \rangle$ and $\langle p_z^2 \rangle$—the mean square momentum projected respectively in the basal plane and along the *c* axis.

beryllium is given by

$$\text{FWHM} = 0.6796(8 \ln 2)^{1/2}(\langle p^2 \rangle / M)^{1/2} Q \tag{5}$$

where Q is in Å^{-1} and $\langle p^2 \rangle / M$ is in meV.

2.3. *The incoherent dynamical structure factor*

We now present the results of a numerical calculation of the exact incoherent dynamical structure factor. Within the harmonic approximation for a cubic Bravais lattice this is given by

$$S^{\text{inc}}(\boldsymbol{Q}, \omega) = \frac{1}{2\pi\hbar} \int_{-\infty}^{\infty} \mathrm{d}t \exp(-\mathrm{i}\omega t) \exp[(\hbar Q^2/2M)(\gamma(t) - \gamma(0))] \tag{6}$$

where

$$\gamma(t) = \int_{-\infty}^{\infty} \mathrm{d}\omega \frac{g(\omega)}{\omega} n(\omega) \exp(-\mathrm{i}\omega t) \tag{7}$$

and $n(\omega)$ is the Bose–Einstein occupation factor (Lovesey 1987). We have further approximated the true incoherent dynamical structure factor of beryllium, which has the HCP structure, by equation (6). This is partly justified by the high degree of isotropy of the atomic vibrations in beryllium, and by the fact that we were only interested in the overall qualitative behaviour of $S^{\text{inc}}(\boldsymbol{Q}, \omega)$ as a function of wave-vector transfer. The computer program containing the fast Fourier transform routines used to evaluate equations (6) and (7) has been described previously (Mayers *et al* 1989). In our calculation of $S^{\text{inc}}(\boldsymbol{Q}, \omega)$ for beryllium we used the normalised phonon density of states given in section 2.2. As the $S^{\text{inc}}(\boldsymbol{Q}, \omega)$ generated using both $g_z(\omega)$ and $g_{xy}(\omega)$ were in close qualitative agreement, we will only present the results using the former. In figure 4 we show a comparison between $S^{\text{inc}}(\boldsymbol{Q}, \omega)$ and the impulse approximation for three values of wave-vector transfer. At $Q = 20\ \text{Å}^{-1}$, sharp features in $S^{\text{inc}}(\boldsymbol{Q}, \omega)$ arising from multi-phonon processes are seen to occur up to an energy transfer of 150 meV. These processes are predicted to produce significant ripples in the lineshape of $S^{\text{inc}}(\boldsymbol{Q}, \omega)$ even at $Q = 30\ \text{Å}^{-1}$. It is only for $Q \gg 30\ \text{Å}^{-1}$ that $S^{\text{inc}}(\boldsymbol{Q}, \omega)$ is calculated to have a smooth, almost Gaussian distribution which is close to the impulse approximation result.

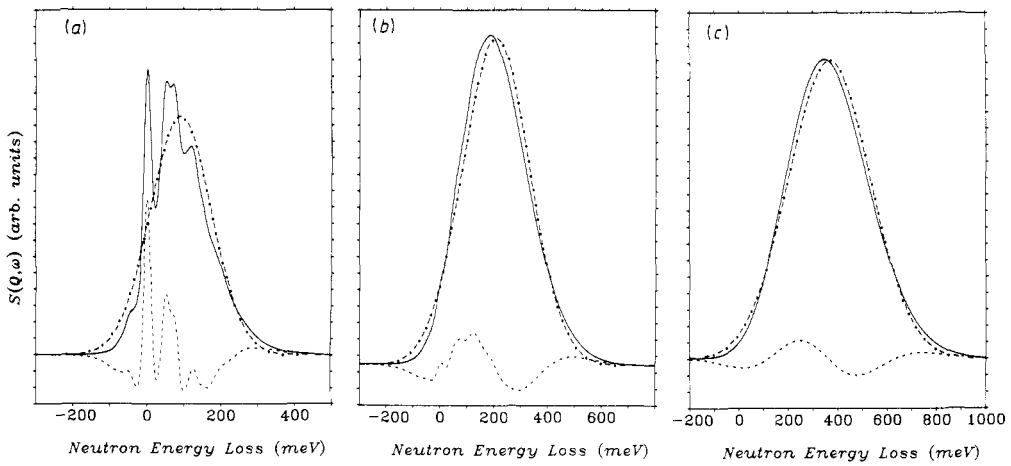

Figure 4. The exact incoherent dynamical structure factor (full curve) calculated from $g_z(\omega)$ compared with the impulse approximation result (chain curve): (*a*) for wave-vector transfer $Q = 20$ Å^{-1}; (*b*) for $Q = 30$ Å^{-1}; (*c*) for $Q = 40$ Å^{-1}. The difference between the two is given by the broken curve.

3. Experimental details

The measurements of the recoil scattering were made on the direct geometry time-of-flight spectrometer HET at ISIS, Rutherford Appleton Laboratory, UK. This instrument was primarily designed to study systems at high energy transfers with low associated wave-vector transfers. The installation of a bank of eleven ^{3}He gas detectors, centred at a scattering angle of 137° and separated from each other by ≈0.4°, has extended its use to problems requiring high energy and high wave-vector transfers. (A full description of HET has been published by Taylor *et al* 1987.) In our experiments we were mainly interested in the results from the high-angle detector array; the detectors covering the lower angles were used to estimate the multiple scattering. The angles of the detectors were calibrated by removing the chopper and observing the scattering from a Ni powder.

In this study we used a large flat-plate single crystal of beryllium, measuring ≈4.5 × 4.0 × 1.3 cm^3 with the *c* axis perpendicular to the largest face. Unfortunately, we cannot give any details of the crystal's growth as it was produced over 20 years ago and has been used as a monochromator crystal in the intervening period at ORNL.

The purpose of our experiments was to study how the recoil scattering from beryllium varied as the wave-vector transfer was aligned along different crystallographic axes. (For a given detector the wave-vector transfer varies in a time-of-flight (TOF) scan, but can be easily calculated from the scattering angle and neutron energy transfer.) The first step in aligning the beryllium crystal was to mount it on a goniometer in the white beam and then orientate it such that the Bragg reflections from the crystallographic planes perpendicular to the desired axis passed into the central detector of the high-angle array. The crystal was then rotated in the (vertical) scattering plane by the amount (≈2°) calculated to bring the required axis along the wave-vector transfer. We note that the direction of the wave-vector transfer corresponding to the centre of the impulse approximation is independent of the incident neutron energy. Consequently, the alignment procedure had only to be carried out once for each axis. We performed three

separate sets of experiments with the wave-vector transfer respectively along ⟨001⟩, ⟨110⟩ and ⟨100⟩, and we estimate that in each case the crystal was aligned to better than 0.5°. With the wave-vector transfer along ⟨001⟩, we collected TOF spectra at various values of the incident neutron energy between 0.13 and 2 eV. Whereas with the wave-vector transfer in the basal plane we restricted our attention to the range of energy between 1 eV and 2 eV.

In a TOF experiment, data are recorded at constant scattering angle φ and we denote the resulting dynamical structure factor by $S_{IA}(\varphi, \omega)$. It has been shown (Jackson 1974) that if the dynamical structure factor at constant wave-vector transfer has a Gaussian distribution then $S_{IA}(\varphi, \omega)$ will, to a first approximation, also be Gaussian. The relationship between the variance σ of the dynamic structure factor at constant wave-vector transfer to the variance σ_φ at constant scattering angle is given by

$$\sigma_\varphi = \sigma\{1 - (m_n/M)[(K_0/K_1)\cos\varphi - 1]\}^{-1} \tag{8}$$

where m_n is the neutron mass, and $\boldsymbol{K}_0$ and $\boldsymbol{K}_1$ are respectively the incident and scattered wave-vectors of the neutron. For our particular scattering geometry $K_0/K_1 \simeq 1.22$ and thus $\sigma_\varphi/\sigma \simeq 0.828$.

To improve the counting statistics, the TOF spectra from all the detectors in the high-angle array were added together after converting the raw data to an energy scale and applying a correction for the energy dependence of the detector efficiency. The resulting scattered neutron energy distribution is directly proportional to the dynamic structure factor at constant scattering angle. The fact that the detectors cover a finite angular range means that the centres of the recoil peaks recorded in each of the detectors were slightly displaced in energy from one another. However, a numerical simulation showed that this systematic broadening of the measured lineshape was negligible compared with the uncertainty in the width arising from counting statistics.

4. Results

At the lowest incident neutron energy used of 0.13 eV, and with the wave-vector transfer along ⟨001⟩, the scattered neutron energy distribution displayed sharp, discrete peaks characteristic of scattering by phonons. As we increased the incident neutron energy the spectral weight gradually shifted from the phonon peaks to a broad excitation situated at a higher neutron energy transfer than the phonon peaks. This broad feature, as we will show, arises predominantly from single-event recoil scattering. Above an incident neutron energy of $\simeq$1 eV the profile of the scattered neutron energy distribution was smooth. A typical spectrum recorded with the neutron wave-vector transfer along ⟨001⟩ for an incident neutron energy well above the transition region is shown in figure 5(*a*). As can be seen from this figure, the measured scattered neutron distribution was highly asymmetric with an appreciable high-energy tail. The intensity of this high-energy tail relative to the peak intensity was found to depend on the orientation of the neutron wave-vector transfer $\boldsymbol{Q}$ with respect to the crystallographic axes; it was much greater with $\boldsymbol{Q}$ applied along ⟨001⟩, when the angle between the incident neutron beam and the surface normal of the beryllium plate was $\simeq$22.5°, than with $\boldsymbol{Q}$ applied either along ⟨100⟩ or ⟨110⟩, when the neutron beam was incident in the plane of the beryllium plate.

We attribute the existence of the high-energy tail to multiple inelastic scattering of the neutron in the sample. The main experimental evidence to support this proposition came from the data collected by the low-angle detectors, which covered the scattering

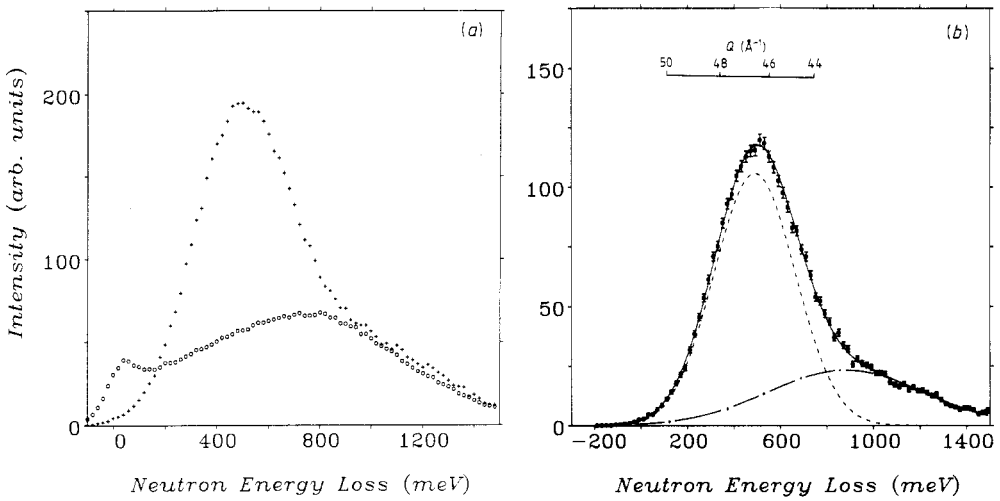

Figure 5. The scattering from single-crystal beryllium at room temperature. (*a*) With the wave-vector transfer along ⟨001⟩ for an incident neutron energy of 1565 meV. The crosses (+) and circles (○) represent respectively the scattering observed in the high- and low-angle detector arrays. The low-angle data have been corrected for the difference in solid angle between the two detector banks. (*b*) With the wave-vector transfer along ⟨110⟩ for an incident neutron energy of 1557 meV. The full curve is a fit to the sum of two Gaussians, one representing single-event recoil scattering (broken curve) and the other multiple inelastic scattering (chain curve), in addition to a flat background.

angles from 3° to 7°. For comparison with the high-angle results, we have also plotted in figure 5(*a*) the low-angle spectrum. The main feature observed in the low-angle data was a broad distribution of intensity centred at approximately twice the neutron energy transfer of the peak observed in the high-angle detector array. This must have originated from multiple inelastic scattering of the neutron in the sample. In addition to this broad feature, there was a significant amount of low-energy scattering from phonons. For the case of $\boldsymbol{Q}$ applied along ⟨001⟩, after correcting for the difference in solid angle between the low- and high-angle detector arrays, the scattering at high neutron energy transfers was found to be very similar in the two detector arrays, as is clearly shown in figure 5(*a*). This fact appears to indicate that the high-energy scattering obtained in the two detector arrays originated from the same physical process, namely multiple inelastic scattering.

In order to test the plausibility of the equivalence of the multiple scattering in the high- and low-angle detector banks, we calculated the neutron scattering cross-section for two-process scattering within the impulse approximation, assuming that the sample was an infinitely thin sheet. For the case of the plate at 22.5° to the incident neutron beam we found that the two-process cross-section for the high- and low-angle detector arrays is very similar, in agreement with our observations. The calculated centre and width of the two-process peak were respectively $\simeq 0.38\,E_0$ and $\simeq 0.32\,E_0$, where E_0 is the incident neutron energy. A comparison of these values with the observed low-angle scattering which had a centre and width both $\simeq 0.5\,E_0$ suggests that high-order multiple scattering is also important.

Further evidence to support our assertion on the origin of the high-energy tail in multiple inelastic scattering processes was provided by an experiment on a thin ($\simeq$2 mm)

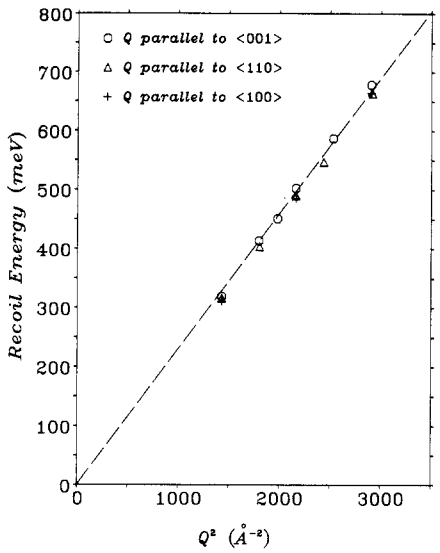

Figure 6. The fitted peak position of the single-event recoil scattering against the square of the wave-vector transfer. The straight line represents the locus of the centre of the recoil scattering calculated from the impulse approximation. The errors in the fitted peak positions are comparable to the size of the symbols.

plate of polycrystalline beryllium. For an incident neutron energy of 1562 meV the observed high-angle spectrum was found to be well described by a single Gaussian.

Unfortunately, because of the intensity of the multiple scattering, we were prevented from achieving one of our main goals in this experiment, which was to try to observe any deviations of the lineshape from a Gaussian form due to final-state interactions.

Having firmly established the cause of the high-energy tail, we then had to decide which was the best method of correcting for its effects. One possibility could have been to subtract the low-angle data from the high-angle data. However, this approach would fail at low energies because the low-angle results have structure arising from scattering by phonons which is absent in the high-angle data. An alternative approach would be to calculate the multiple scattering in detail, but since this involves many scattering processes, the results would not be adequate in detail. The approach we finally adopted was to fit the measured high-angle spectra to the sum of two Gaussians, one representing single-event recoil scattering and the other multiple-event recoil scattering. The result of such a fit to a spectrum with $\boldsymbol{Q}$ along $\langle 110 \rangle$ is shown as a full curve in figure 5(*b*). (Typically the reduced χ^2 in our fits varied between 1.0 and 1.5.) An important check that our assumption of a Gaussian form for the multiple scattering did not introduce any gross errors into the fitted values of the centre and width of the single-event recoil scattering was provided by a comparison of the polycrystalline and single-crystal results. The scattering from the polycrystalline sample was successfully fitted to a single Gaussian with a centre and width which differed from the single-crystal results by only 0.6% and 3% respectively.

The values of the centre of the single-event recoil peak from the two-Gaussian fits are plotted in figure 6 as a function of Q^2, for all three orientations of the beryllium crystal. On the same figure, the recoil energy E_r given by the impulse approximation is plotted as a broken line.

The fitted values of the FWHM of $S_{IA}(\varphi, \omega)$ are shown in figure 7 as a function of Q. (For clarity we have separated the results obtained for $\boldsymbol{Q}$ in the basal plane from those with $\boldsymbol{Q}$ along *c*.) We have corrected for the effects of finite instrumental resolution by

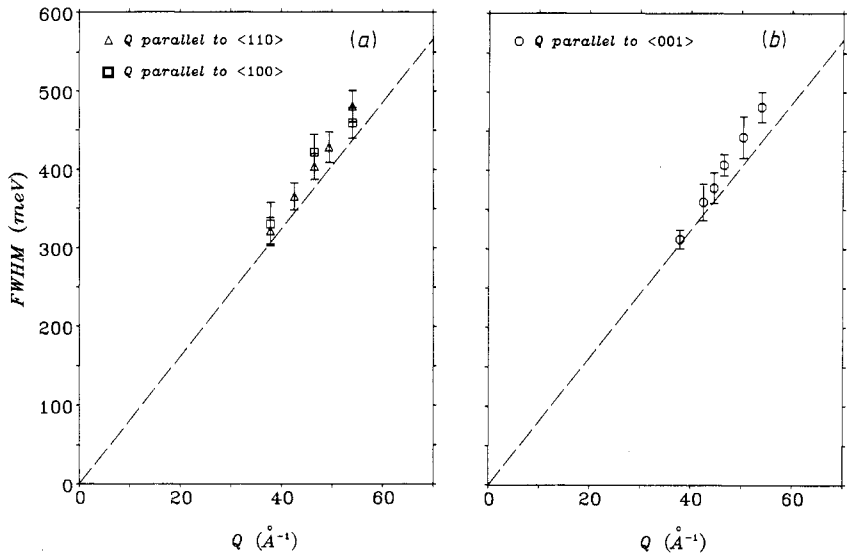

Figure 7. The fitted widths (FWHM) of the single-event recoil scattering against wave-vector transfer: (*a*) with the wave-vector transfer in the basal plane along ⟨110⟩ and ⟨100⟩; (*b*) with the wave-vector transfer along ⟨001⟩. The broken line was obtained from the calculated mean squared momentum derived by fitting a Born–von Karman model to the measured phonon dispersion relations.

assuming that the measured distribution is a convolution of a Gaussian $S_{IA}(\varphi, \omega)$ with a Gaussian resolution function. The energy resolution of HET for our particular experimental configuration was $\simeq 1.6\%$ of the incident neutron energy (Taylor *et al* 1987). Although the resolution function is not strictly a Gaussian, we believe that this procedure gives widths that are accurate to within the estimated errors.

5. Discussion

From figure 6 we see that for the measurements with the wave-vector transfer along ⟨001⟩ the recoil scattering is centred, within experimental error, on the recoil line given by the impulse aproximation for $Q \gtrsim 35$ Å^{-1}. This is in agreement with our calculation of the asymptotic behaviour of the exact incoherent structure factor presented in section 2.3. However, in the case of the corresponding data sets with the wave-vector transfer in the basal plane, the centre of the scattering is slightly, but systematically, depressed from the recoil line. There are two possible explanations for this discrepancy: either it is a real effect, produced by a difference in the final-state interactions between atoms recoiling within the basal plane and those recoiling along *c*; or it is an artefact, arising from our method of correcting for the effects of multiple inelastic scattering. As far as the former is concerned, in the HCP structure of beryllium final-state interactions are expected to play a more dominant role for scattering within the basal plane, as here an atom has a shorter distance to travel before colliding with one of its nearest neighbours than when it is scattered along *c*. In the latter case, as a consequence of the slab geometry of our sample, there was a difference in the intensity of multiple inelastic scattering of

about a factor of two between having $\boldsymbol{Q}$ along $\boldsymbol{c}$ and in the basal plane. This may have led to a systematic error in the fitted centre of the single-event recoil scattering. Clearly, to choose between these two possible explanations further experiments are required on a small single crystal, the geometry of which could be selected to reduce multiple-scattering processes to a minimum. This is, however, currently unfeasible as it would require excessive neutron beam time.

In figure 7 we see that the measured FWHM of the recoil scattering increases smoothly and linearly with Q, and there is no evidence for the oscillations that have been observed in liquid helium (Martel *et al* 1976) and liquid neon (Buyers *et al* 1975). Its magnitude is in reasonable agreement with the value calculated from the $\langle p^2 \rangle$ obtained from the phonon density of states given in section 2.2 for all three orientations of the wave-vector transfer. The tendency of most of the experimental data to lie slightly above the theoretical values may be due to the inadequacy of our assumption that the instrumental resolution is Gaussian over the entire range of incident neutron energy used in the experiment. In general, it can be expected that this approximation will be less valid at higher values of the incident neutron energy. This agrees with the observed trend for the difference between the experimental and theoretical values to increase with Q. The fact that the observed FWHM is in agreement with the value calculated from a harmonic model of beryllium is consistent with the results of a neutron diffraction study of beryllium by Larsen *et al* (1980), who found that the anharmonic contributions to the Debye–Waller factor were small at room temperature.

In conclusion, we have established from studying the position of the centre of the recoil scattering from beryllium that the impulse approximation is approached, within experimental error, for $Q \geqslant 35$ Å^{-1}. We have further shown that our empirical criterion for the validity of the impulse approximation is consistent with the results of numerical calculation of the asymptotic behaviour of the exact incoherent dynamic structure factor. Although the measured FWHM of the recoil scattering for $Q \geqslant 35$ Å^{-1} agrees with the value calculated from the density of states generated using a harmonic model of beryllium, the calculated value itself does not depend strongly on the details of the density of states. In fact our measurements are also consistent with a Debye model. Thus we feel it is unlikely that, for systems interacting via potentials that are largely harmonic in nature, the type of experiment described in this paper will provide any new information that is not better obtained using other techniques.

Acknowledgments

We would like to thank Mark Hewitt for helpful discussions, Jerry Mayers for allowing us to use his computer program to calculate the incoherent dynamic structure factor, Ray Osborn for his help with the data analysis programs and R Steadman for making available to us his phonon data. We also gratefully acknowledge the hospitality of the staff of the Rutherford Laboratory and Ridgeway House.

References

Buyers W J L, Sears V F, Lonngi P A and Lonngi D A 1975 *Phys. Rev.* A **11** 697–712
Gunn J M F, Andreani C and Mayer J 1986 *J. Phys. C: Solid State Phys.* **19** L835–40
Gunn J M F and Warner M 1984 *Z. Phys.* B **56** 13–20

Hewitt M, Cowley R A and Taylor A D 1989 to be published
Hilleke R O, Chaddah P, Simmons R O, Price D L and Sinha S K 1984 *Phys. Rev. Lett.* **52** 847–50
Hohenberg P C and Platzman P M 1966 *Phys. Rev.* **152** 198–200
Houmann J C G and Nicklow R M 1970 *Phys. Rev.* B **1** 3943–52
Jackson H W 1974 *Phys. Rev.* A **10** 278–94
Larsen F K, Lehmann M S and Merisalo M 1980 *Acta Crystallogr.* A **36** 159–63
Lovesey S W 1987 *Theory of Neutron Scattering from Condensed Matter* vol 1 (Oxford: Oxford University Press)
Martel P, Svensson E C, Woods A D B, Sears V F and Cowley R A 1976 *J. Low Temp. Phys.* **23** 285–301
Mayers J, Andreani C and Baciocco G 1989 *Phys. Rev.* B **39** 2022–8
Sears V F 1969 *Phys. Rev.* **185** 200–6
—— 1984 *Phys. Rev.* B **30** 44–51
Silver R N 1988 *Phys. Rev.* B **37** 3794–7
Steadman R, Amilius Z, Pauli R and Sundin O 1976 *J. Phys. F: Met. Phys.* **6** 157–66
Taylor A D, Boland B C, Bowden B C and Jones T J L 1987 *Rutherford Appleton Laboratory Report* RAL-87-012
Weinstein J J and Negele J W 1982 *Phys. Rev. Lett.* **49** 1016–19